PHYSICAL REVIEW B **78**, 180406(R) (2008)

Doping-dependent charge and spin superstructures in layered cobalt perovskites

N. Sakiyama,[1] I. A. Zaliznyak,[2,*] S.-H. Lee,[3] Y. Mitsui,[1] and H. Yoshizawa[1]
[1]*Neutron Science Laboratory, Institute for Solid State Physics, University of Tokyo, Tokai 319-1106, Japan*
[2]*DCMPMS, Brookhaven National Laboratory, Upton, New York 11973, USA*
[3]*Department of Physics, University of Virginia, Charlottesville, Virginia 22904, USA*
(Received 7 October 2008; published 12 November 2008)

We have investigated cobaltite relatives of the layered perovskite cuprates and nickelates, $Pr_{2-x}Ca_xCoO_4$ ($0.39 \leq x \leq 0.73$) and $La_{2-x}Sr_xCoO_4$ ($x=0.4, 0.61$), using elastic neutron scattering. We have discovered doping-dependent incommensurate short-range ordering of charges and magnetic moments, which in cobaltites occur in the nonitinerant polaron phase, for $0.5 \lesssim x \lesssim 0.75$. The charge order exists already at room temperature and shows no change on cooling. The incommensurability of its propagation vector, $\mathbf{Q}_c=(\epsilon_c, 0, l)$, roughly scales with the concentration of Co^{2+} ions, $\epsilon_c \sim (1-x)$. Magnetic order follows at low $T \lesssim 40$ K and has twice larger periodicity, indicating a dominant antiferromagnetic correlation between the nearest Co^{2+} spins.

DOI: 10.1103/PhysRevB.78.180406 PACS number(s): 75.70.Cn, 71.27.+a, 71.28.+d, 71.30.+h

Physical origins of doping-dependent incommensurate charge and spin orderings (CO and SO) in doped Mott-Hubbard insulators (MHI) and their relevance to the mechanisms of high-temperature superconductivity in cuprates still remain a mystery. Numerous experiments have shown that doped holes in $La_{2-x}Sr_xCuO_4$ cuprates and closely related isostructural but insulating doped layered perovskite nickelates, $La_{2-x}Sr_xNiO_4$, exhibit an in-plane CO whose propagation vector is roughly proportional to doping x and magnetic order, whose modulation period is twice larger.[1–8] One simple picture of such simultaneous real-space ordering of charges and spins is provided by the charge stripe model, where itinerant doped holes segregate into lines separating stripes of antiferromagnetic domains.[1] It is supported by the theoretical analysis of the two-dimensional (2D) Hubbard model, which is believed to describe high-T_c cuprates, and an influential school of thought advocates that electronic nematic phase in the form of charge stripes in fact promotes superconductivity in doped cuprates.[3,9–12] The key point in such a picture is that doped holes are highly mobile so one-dimensional (1D) delocalization decreases their kinetic energy. Charge and antiferromagnetic spin orders in this model are intimately coupled, as both are signatures of the same ordering instability of interacting itinerant charges in 2D MHI, arguably aiding superconductivity rather than competing with it.

However, most MHI cannot even be made metallic by doping, as strong polaronic self-localization of doped charges hinders metallic transport.[13] The above itinerant stripe picture discards such charge immobilization effects. While this is justified for moderately to highly doped cuprates with "parallel" (aligned with Cu-O bonds) stripes and metallic conductivity,[14] it is questionable for lightly doped cuprates and insulating nickelates, where CO implies "diagonal" stripes with charge lines at 45° to Cu-O bonds and activated charge transport.[13,15] Doping-dependent diagonal CO (but not SO), with incommensurability $\delta \sim 1-x$, was also found in perovskite manganites, where it competes with metallic behavior, yielding an insulating phase for $x \gtrsim 0.5$.[16–19] Complex interplay of double exchange, lattice interactions, and orbital degeneracy in this case lead to a number of conflicting interpretations of CO, ranging from stripes to Wigner crystal to polaronic charge-density wave. So, is it possible to disentangle the relative importance of itinerancy and various interactions in driving doping-dependent charge and spin orders with SO and CO incommensurabilities related by $\delta_s \sim \epsilon_c/2$ in doped MHI?

In an attempt to answer this question we have studied layered perovskite cobalt oxides $Pr_{2-x}Ca_xCoO_4$ (PCCoO), $0.39 \leq x \leq 0.73$, and $La_{2-x}Sr_xCoO_4$ (LSCoO), $0.4 \leq x \leq 0.61$, which are isostructural with 2D cuprates and nickelates, but have different $3d^7/3d^6$ local electronic configuration of Co^{2+}/Co^{3+}.[20] Despite this superficial complication, cobaltites actually represent rather simple limit, one where polaronic effects clearly dominate, leading to nonitinerant behavior of doped charges.[20–23] Their undoped ($x=0$) parent materials are also antiferromagnetic insulators [$T_N \approx 275$ K for LSCoO (Ref. 21)], but unlike cuprates or manganites, layered cobaltites remain insulating throughout the doping range $0 \leq x \lesssim 1$,[23,24] which is in fact typical for a MHI. Theoretically, doping-dependent CO can also occur in MHI with self-localized doped charges, where it is a cooperative ordering of lattice polarons, minimizing lattice strain.[13,25] Short-range checkerboard charge order (CCO) observed by neutron diffraction in the $x=0.5$ LSCoO sample at $T \lesssim 825$ K (Ref. 22) is perhaps such a correlated polaron glass phase although CCO can also be viewed as a limiting case of charge stripe order with shortest possible stripe spacing, and this is how it was interpreted in the $x=0.5$ nickelate.[6,7] In LSCoO, however, CO is totally independent of spins, which only order at $T \lesssim 30$ K, and detailed investigation of SO scattering revealed no evidence for incipient 1D charge stripes.[26]

Holes in doped cobaltites are strongly localized. The ab-plane resistivity in LSCoO is in the ~ 10 Ω cm ($x=1$) to $\gtrsim 10^4$ Ω cm ($x \lesssim 0.5$) range and shows polaronic activated behavior with activation energy $E_a \sim 1500$ K to $E_a \gtrsim 5000$ K, respectively.[23] Electrical resistivity and thermal activation energy measured by Physical Property Measurement System (Quantum Design Co.) in our PCCoO single-crystal samples are shown in Fig. 1(a). Samples were grown by the floating zone method and their uniformity was verified by scanning electron microscopy. The actual chemical composition x was then determined using the inductively coupled plasma method. The absence of impurity phases was con-

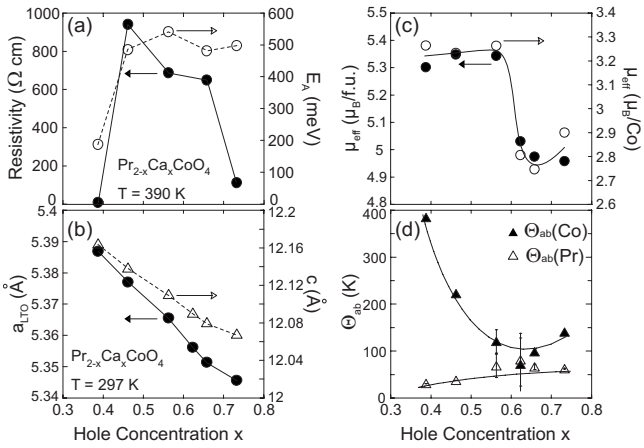

FIG. 1. Doping dependence of electrical, structural, and magnetic properties of PCCoO. Missing error bars are smaller than symbol size; lines are guide for the eyes. (a) Resistivity at the highest measured temperature (closed symbols) and its activation energy (open). (b) $F4/mmm$ (LTO) lattice parameters refined at room temperature by powder x ray. (c) Effective magnetic moment μ_{eff} per formula unit obtained by one-component Curie-Weiss analysis of the in-plane magnetic susceptibility $\chi_{ab}(T)$, 50 K$\leq T \leq$300 K, which includes Pr^{3+} contribution (left scale, closed symbols). Open symbols are μ_{eff} per Co ion obtained from two-component Curie-Weiss fit with fixed $\mu_{\text{eff}}^{\text{Pr}}=3.58\mu_B$; (d) corresponding Weiss temperatures for Co (filled) and Pr (open). Nonzero Θ_{ab}(Pr) is likely within the limits of the systematic error of such analysis.

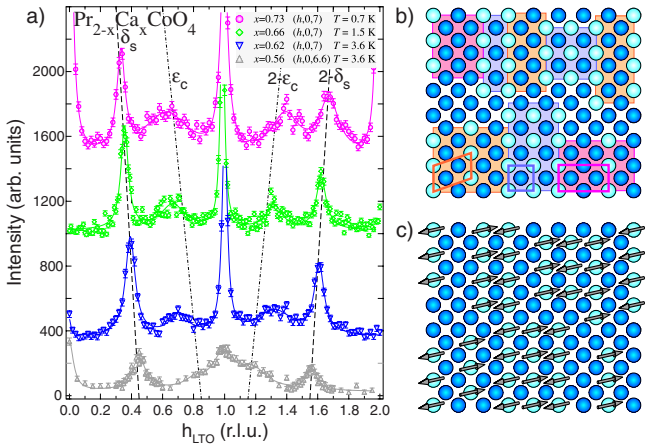

FIG. 2. (Color online) (a) Elastic scans along $(h,0,7)$ or $(h,0,6.6)$, showing charge and spin order peaks at $\mathbf{Q}_c=(2n\pm\epsilon_c,0,l)$ and $\mathbf{Q}_s=(2n\pm\delta_s,0,l)$, respectively. Solid lines are Lorentzian fits; broken lines trace $\epsilon_c\simeq 2\delta_s$. Peak at (007) contains superlattice Bragg intensity resulting from the LTO distortion but is contaminated by lattice Bragg scattering of $\lambda/2$ neutrons. (b) Sketch of glassy charge-ordered state with a mixture of different commensurate superlattice fragments accommodating the nominal doping $x\approx 0.7$; (c) antiferromagnetic correlations governed by $Co^{2+}-Co^{3+}-\cdots-Co^{2+}$ superexchange between Co^{2+} spins (arrows) developing in this CO state.

firmed by powder x-ray diffraction. Samples were further characterized by measuring static magnetic susceptibility by superconducting quantum interference device magnetometer. Typical data are presented in the inset of Fig. 4(b). Weiss temperature Θ_W and Co effective magnetic moment resulting from the Curie-Weiss analysis of its T dependence are shown in Figs. 1(d) and 1(c).

For neutron-diffraction studies we used $\approx$20 mm long $\phi\approx 6$ mm cylindrical single-crystal pieces of $m\approx 2$ g. Mosaic of the fundamental Bragg reflections was $\lesssim 0.5°$, which is consistent with the instrumental resolution and shows high crystalline quality. Neutron experiments were performed on 4G and 5G three-axis thermal-neutron spectrometers at the JRR-3 at JAEA, Tokai, Japan, with $40'-40'-40'-40'$ beam collimation and BT9 spectrometer at the NIST Center for Neutron Research, with beam collimation $\approx 40'-47'-44'-80'$ (open). Wave vector of the incident and scattered neutrons was selected by the (002) Bragg reflection from pyrolitic graphite (PG) and fixed at $k_i\simeq 2.67$ Å. Contamination from higher order reflections was suppressed by 1–2 in. thick PG transmission filters. Sample was mounted in a closed-cycle He gas refrigerator with a-b plane vertical and $(h0l)$ reciprocal-lattice zone in the horizontal scattering plane. We index wave vectors in the $F4/mmm$ lattice with the unit cell $\sqrt{2}a\times\sqrt{2}a\times c$ compared to the $I4/mmm$ high-temperature tetragonal lattice of cuprates with $a\approx 3.8$ Å. We assign low-temperature orthorombic (LTO) index to the in-plane lattice parameters thus defined, Fig. 1(b), since our samples are actually in the LTO phase, but the orthorombic distortion is way too small to be resolved in the present measurements.[26]

Typical low-temperature scans along h_{LTO} direction, revealing superlattice scattering in several PCCoO samples are shown in Fig. 2. Two sets of peaks whose position varies roughly linearly with doping can be identified. Sharper and more intense peaks at $\boldsymbol{Q}_s=\boldsymbol{G}\pm(\delta_s,0,l)$, where $\boldsymbol{G}$ is the wave vector of a fundamental lattice Bragg reflection, quickly disappear upon heating to $T\gtrsim 40$ K and decrease in intensity with increasing Q_s for different $\boldsymbol{G}$, consistent with the square of the Co^{2+} magnetic form factor. Hence, we identify these peaks as magnetic scattering arising from spin order. Their position varies roughly linearly with the remaining Co^{2+} content, $\delta_s(x)\sim(1-x)$. Weak diffuse peaks at $\boldsymbol{Q}_c=\boldsymbol{G}\pm(\epsilon_c,0,l)$, whose position varies roughly as $\epsilon_c(x)\sim 2(1-x)$, are much broader and in fact increase in intensity with increasing Q_c in different $\boldsymbol{G}$ zones, roughly $\sim Q_c^2$. We therefore identify them as superstructural scattering arising from atomic displacements accompanying short-range charge (valence) order. These peaks remain unchanged both in width and intensity upon heating to $T\approx 300$ K.

Strong peak at (1,0,7) is consistent with Bragg scattering arising from the LTO lattice distortion. Its intensity grows rather gradually below $\approx$300 K and then usually decreases below $T\sim 100$ K. Similar peak is present at $l=6$ and other integer l. This type of reflections was observed by neutron diffraction in the undoped La_2CoO_4.[21] As $x\to 0.5$, $\epsilon_c(x)\to 1$, and LTO Bragg scattering at $h=1$ overlaps with weak CO peaks at $\boldsymbol{G}\pm\boldsymbol{Q}_c$. The latter, however, persist to much higher temperature, T$\sim$700–800 K, and are much broader. The lower scan in Fig. 2(a) for $x=0.56$ was performed at $l=6.6$ and has only weak peak at $h=1$, while incommensurate CO peaks are practically unchanged compared to $l=7$.

The l dependence of CO scattering measured in our samples shows no peaks due to interplane coherence

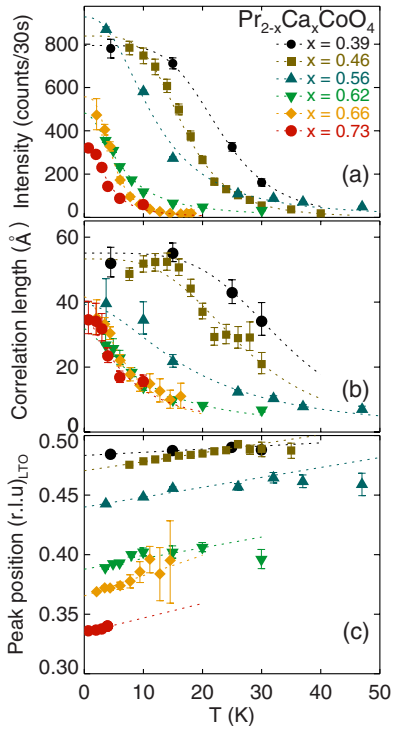

FIG. 3. (Color online) Temperature dependence of magnetic SO peak parameters in PCCoO. (a) Peak intensity cross normalized to ≈30 s BT9 monitor count for equal sample mass; (b) in-plane correlation length ξ_{ab} [inverse half-width at half maximum (HWHM) of Lorentzian fit]; (c) peak position.

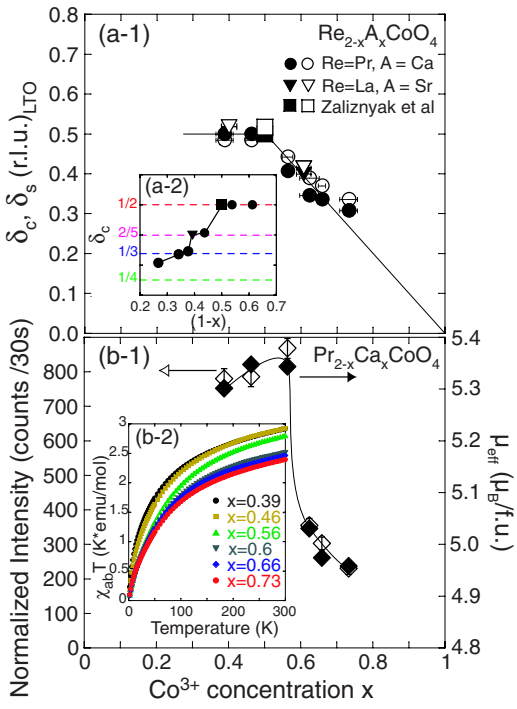

FIG. 4. (Color online) (a) Diagram of the propagation vector for spin and charge superstructures in PCCoO and LSCoO. Filled (open) symbols show the in-plane modulation vector for charge (spin) order, $\delta_c=\epsilon_c/2$ and δ_s, respectively. Inset (a)-(2) is the enlarged Yamada-type (Ref. 2) plot showing the lattice commensurability effect on the position of CO peaks at $(2\delta_c,0,l)$. (b) Concentration dependence of μ_{eff} (filled symbols) and peak magnetic neutron scattering intensity (open) in PCCoO. Inset (b)-(2) shows $T\chi_{ab}$ for selected x's. Missing error bars are smaller than symbol size; lines are guide for the eyes.

$(\xi_c^l \lesssim 0.2c)$, but smooth intensity variation resembling that reported for $x=0.5$ LSCoO.[22] This indicates that scattering arises from similar distortions of CoO_6 octahedra associated with charge-lattice small polarons. In $x=0.39, 0.46$ PCCoO and $x=0.4$ LSCoO samples, CO peak is at $h=1$, indicating finite region of stability of the CCO phase at $x\leq 0.5$. The in-plane peak width in these samples is similar to that in $x=0.5$ LSCoO, corresponding to CCO correlation length ξ_c^h of three to five LTO lattice units. For $x\geq 0.5$, where charge correlations are incommensurate, CO peaks are at least twice broader, corresponding to $\xi_c^h \lesssim 10$ Å. Despite different tolerance factors and bandwidths compared to PCCoO, $x=0.61$ LSCoO sample shows very similar glassy CO and SO correlations, which follow the same doping trend.

The picture of CO at $x\geq 0.5$ arising from these observations is illustrated in Fig. 2(b). Polarons associated with Co^{2+} sites, whose concentration is $n_e=1-x$, build up patches of commensurate superlattices corresponding to $n_e=1/2, 1/3, 1/4$, etc., where particular n_e is locally favored by La/Sr doping fluctuation. Their long-range coherence, however, is frustrated by the charge neutrality condition imposed by the average Sr^{2+} concentration x. Hence, glassy CO state results, which is made of a mixture of ~1 nm sized domains of commensurate polaron superlattices, accommodating the average charge doping. Consequently, CO scattering has an average incommensurability of $\epsilon_c(x)\approx 2(1-x)$.

Magnetic SO scattering with roughly half the CO incommensurability simply corresponds to the antiferromagnetic order of Co^{2+} spins [Fig. 2(c)]. Magnetic correlations are apparently governed by $Co^{2+}-Co^{3+}-\cdots-Co^{2+}$ superexchange (note that $\Theta_W>0$ for all x [Fig. 1(d)]. They decrease with increasing number of intervening Co^{3+}, but also extend between the different CO superlattice domains, which explains why the in-plane SO correlation length ξ_s^h is three to four times larger than ξ_c^h. This also explains the decrease with x of the SO temperature seen in panel (a) of Fig. 3, which shows the T dependence of the SO peak parameters. Typical of a glassy spin freezing, SO peak intensity increases smoothly with decreasing T, while the correlation length ξ_s^h [Fig. 3(b)] increases and seems to saturate roughly where the intensity reaches half its maximum. The temperature dependence of the SO peak position [Fig. 3(b)] also shows an interesting trend, which can be simply understood in this model. Indeed, as longer-periodic CO polaron superlattices present in a given sample gradually develop spin correlations with decreasing T, the average magnetic modulation period becomes longer and $\delta_s(T)$ decreases. Similar to the CCO case in $x=0.5$ LSCoO, CO is totally uncoupled from SO, which simply follows the CO-induced superexchange pattern.

The doping dependencies of the incommensurabilities of charge and spin orders are summarized in Fig. 4(a). As mentioned before, for $x\geq 0.5$ both roughly follow the $\sim 1-x$ trend although $\delta_s(x)$ is always somewhat larger than $\epsilon_c(x)/2$,

corresponding to shorter average SO modulation period. This again is consistent with the picture where shorter-periodic polaron superlattices have better developed spin correlations. Detailed investigation of the CO peak position [Fig. 4(a)-(2)] shows lattice commensurability effect on CO, indicating that most observed CO peaks can be assigned to a mixture of two nearest commensurate superlattices.[6,7]

Finally, we comment on an apparent doping-induced Co spin state change, which is manifested by a decrease of $\mu_{\mathrm{eff}}(x)$ and in PCCoO occurs at $x \gtrsim 0.56$ [Fig. 1(c)]. Comparison of Figs. 4(a) and 4(b) suggests that other than decrease in the SO peak magnitude coincident with that of μ_{eff} it does not have any significant effect on charge and spin orderings.

In summary, we have discovered doping-dependent charge and spin modulations in PCCoO and LSCoO, whose periods vary roughly linearly with doping, $\delta_s \sim \epsilon_c/2 \sim 1-x$, existing for $x > 0.5$. They border the checkerboard CO phase at $x \lesssim 0.5$. In cobaltites CO occurs in a phase where electrons are strongly localized and can therefore be understood as a correlated polaron glass with nanoscale patches of commensurate CO superlattices, whose long-range coherence is frustrated by the charge neutrality requirement. Antiferromagnetic SO correlations between the nearest "undoped" Co^{2+} sites develop at temperatures more than ten times smaller than CO and do not affect it. Similar CO (but not SO) was found in manganites, where it is driven by orbital degeneracy, Jahn-Teller, and double-exchange physics,[16–19] as well as in cuprates and nickelates, where charge itinerancy is believed to be an important player. Having in many respects quite similar appearance to CO and SO in cuprates, nickelates, and manganites, CO and SO in cobaltites allow to disentangle effects of charge itinerancy and various interactions. Here, they are mainly governed by the lattice electrostatics and the superexchange.

We thank T. J. Sato and K. Hirota for help with experiments and J. Tranquada for discussions. This work was supported by Grants-In-Aid for Scientific Research (C) (Grant No. 16540307) from the Ministry of Education, Culture, Sports, Science, and Technology, Japan, and by the U.S. DOE under Contract No. DE-AC02-98CH10886.

*Corresponding author; zaliznyak@bnl.gov

[1] J. M. Tranquada, B. J. Sternlieb, J. D. Axe, Y. Nakamura, and S. Uchida, Nature (London) **375**, 561 (1995).
[2] K. Yamada, C. H. Lee, K. Kurahashi, J. Wada, S. Wakimoto, S. Ueki, H. Kimura, Y. Endoh, S. Hosoya, G. Shirane, R. J. Birgeneau, M. Greven, M. A. Kastner, and Y. J. Kim, Phys. Rev. B **57**, 6165 (1998).
[3] S. A. Kivelson, I. P. Bindloss, E. Fradkin, V. Oganesyan, J. M. Tranquada, A. Kapitulnik, and C. Howald, Rev. Mod. Phys. **75**, 1201 (2003).
[4] C. H. Chen, S.-W. Cheong, and A. S. Cooper, Phys. Rev. Lett. **71**, 2461 (1993).
[5] J. M. Tranquada, J. E. Lorenzo, D. J. Buttrey, and V. Sachan, Phys. Rev. B **52**, 3581 (1995).
[6] H. Yoshizawa, T. Kakeshita, R. Kajimoto, T. Tanabe, T. Katsufuji, and Y. Tokura, Phys. Rev. B **61**, R854 (2000).
[7] R. Kajimoto, K. Ishizaka, H. Yoshizawa, and Y. Tokura, Phys. Rev. B **67**, 014511 (2003).
[8] S.-H. Lee, J. M. Tranquada, K. Yamada, D. J. Buttrey, Q. Li, and S.-W. Cheong, Phys. Rev. Lett. **88**, 126401 (2002).
[9] J. Zaanen and O. Gunnarsson, Phys. Rev. B **40**, 7391 (1989).
[10] V. J. Emery and S. A. Kivelson, Physica C **209**, 597 (1993).
[11] L. P. Pryadko, S. A. Kivelson, V. J. Emery, Y. B. Bazaliy, and E. A. Demler, Phys. Rev. B **60**, 7541 (1999).
[12] M. Ichioka and K. Machida, J. Phys. Soc. Jpn. **68**, 4020 (1999).
[13] J. Zaanen and P. B. Littlewood, Phys. Rev. B **50**, 7222 (1994).
[14] N. Ichikawa, S. Uchida, J. M. Tranquada, T. Niemöller, P. M. Gehring, S.-H. Lee, and J. R. Schneider, Phys. Rev. Lett. **85**, 1738 (2000).
[15] V. I. Anisimov, M. A. Korotin, J. Zaanen, and O. K. Andersen, Phys. Rev. Lett. **68**, 345 (1992).
[16] C. H. Chen, S.-W. Cheong, and H. Y. Hwang, J. Appl. Phys. **81**, 4326 (1997).
[17] R. Wang, J. Gui, Y. Zhu, and A. R. Moodenbaugh, Phys. Rev. B **61**, 11946 (2000).
[18] W. Bao, C. H. Chen, S. A. Carter, and S.-W. Cheong, Solid State Commun. **98**, 55 (1996).
[19] S. Larochelle, A. Mehta, L. Lu, P. K. Mang, O. P. Vajk, N. Kaneko, J. W. Lynn, L. Zhou, and M. Greven, Phys. Rev. B **71**, 024435 (2005).
[20] Magnetic Co^{2+} are in $3d^7$ ($t_{2g}^5 e_g^2$) state and, like Cu^{2+}, are Kramer's ions, albeit with spin $S=3/2$. Hund's coupling in cobaltites is in close competition with crystal field (CF), so doped holes can yield Co^{3+} ($3d^6$) in an intermediate (IS, $S=1$) or low spin (LS, $S=0$) state (Refs. 22 and 23). Magnetic susceptibility data of Ref. 23 indicate change to a lower-spin Co^{3+} state with doping at $x \sim 0.7$. In either case the ground state in the crystal field is $S^z=0$ singlet and is effectively nonmagnetic at low T (Ref. 22). This is a fundamental consequence of Kramers time-reversal symmetry and makes comparison with cuprates particularly meaningful: Hund's rule is not at play for a single hole in $3d^9$ Cu^{2+}, while covalency and strong correlation yield a non-Hund $S=0$ singlet $3d^8$ state for doped holes.
[21] K. Yamada, M. Matsuda, Y. Endoh, B. Keimer, R. J. Birgeneau, S. Onodera, J. Mizusaki, T. Matsuura, and G. Shirane, Phys. Rev. B **39**, 2336 (1989).
[22] I. A. Zaliznyak, J. P. Hill, J. M. Tranquada, R. Erwin, and Y. Moritomo, Phys. Rev. Lett. **85**, 4353 (2000); I. A. Zaliznyak, J. M. Tranquada, R. Erwin, and Y. Moritomo, Phys. Rev. B **64**, 195117 (2001).
[23] Y. Moritomo, K. Higashi, K. Matsuda, and A. Nakamura, Phys. Rev. B **55**, R14725 (1997).
[24] T. Matsuura, J. Tabuchi, J. Mizusaki, S. Yamaguchi, and K. Fueki, J. Phys. Chem. Solids **49**, 1403 (1988).
[25] D. I. Khomskii and K. I. Kugel, Phys. Rev. B **67**, 134401 (2003); Europhys. Lett. **55**, 208 (2001).
[26] A. T. Savici, I. A. Zaliznyak, G. D. Gu, and R. Erwin, Phys. Rev. B **75**, 184443 (2007).